Catalysis Today 420 (2023) 114001

Contents lists available at ScienceDirect

Catalysis Today

journal homepage: www.elsevier.com/locate/cattod

Selective denitrification of simulated oily wastewater by oxidation using Janus-structured carbon nanotubes

Fernanda F. Roman [a,b,c,d], Jose L. Diaz de Tuesta [e], Flávia K.K. Sanches [a,b,f], Adriano Santos Silva [a,b,c,d], Pricila Marin [f], Bruno F. Machado [c,d,g], Philippe Serp [h], Marta Pedrosa [c,d], Adrián M.T. Silva [c,d], Joaquim L. Faria [c,d], Helder T. Gomes [a,b,*]

[a] Centro de Investigação de Montanha (CIMO), Instituto Politécnico de Bragança, Campus de Santa Apolónia, 5300-253 Bragança, Portugal
[b] Laboratório Associado para a Sustentabilidade e Tecnologia em Regiões de Montanha (SusTEC), Instituto Politécnico de Bragança, Campus de Santa Apolónia, 5300-253 Bragança, Portugal
[c] LSRE-LCM – Laboratory of Separation and Reaction Engineering – Laboratory of Catalysis and Materials, Faculty of Engineering, University of Porto, Rua Dr. Roberto Frias, 4200-465 Porto, Portugal
[d] ALiCE – Associate Laboratory in Chemical Engineering, Faculty of Engineering, University of Porto, Rua Dr. Roberto Frias, 4200-465 Porto, Portugal
[e] Department of Chemical and Environmental Technology, Rey Juan Carlos University, Calle Tulipán s/n., 28933 Móstoles, Spain
[f] Universidade Tecnológica Federal do Paraná, Campus Londrina, 86036-370 Londrina, Brazil
[g] CoLAB Net4CO$_2$- Network for a Sustainable CO$_2$ Economy, Rua Dr. Julio de Matos 828–882, 4200-355 Porto, Portugal
[h] Laboratoire de Chimie de Coordination, ENSIACET, Université de Toulouse, France

ARTICLE INFO

Keywords:
4-nitrophenol
Biphasic oxidation
Fenton-like system
Nanostructured carbons
Janus particles

ABSTRACT

The intense industrial development has resulted in several consequences for human and environmental health, including the increased discharge of oily products in water bodies. Oily products are widely used in industry, often bearing an associated high cost. Finding alternatives to treat oily wastewater aiming at recovering oily and water phases is an approach allowing recovery of products of economic interest. In this work, Janus-like carbon nanotubes (CNTs) were synthesized by varying the feed time of acetonitrile and ethylene, respectively, as nitrogen/carbon and carbon precursors in a chemical vapor deposition (CVD) approach. The CVD approach allowed the synthesis of completely undoped, completely doped and partially doped CNTs with a Janus structure. The CNTs were then tested as catalysts for the selective oxidation of 4-nitrophenol (4-NP) contained in a simulated oily wastewater (2,2,4-trimethylpentane/water (O/W) = 1:9, volume basis) by catalytic wet peroxide oxidation (CWPO). The CWPO experiments were conducted for 24 h, 80 °C, 2.5 g L^{-1} of catalyst, and the stoichiometric concentration of H_2O_2 (3.6 g L^{-1}) for the degradation of 4-NP (1 g L^{-1}). The same conditions were kept for experiments conducted under a biphasic system. The catalysts bearing a Janus-like structure were demonstrated to be more effective in CWPO experiments in aqueous-only and biphasic systems for the abatement of 4-NP.

1. Introduction

The intense industrial development observed in the last decades, primarily related to the extraction and refining of petroleum-based products, has led to an increased deposition of oily compounds in waterbodies, creating effluents referred to as oily wastewater [1]. The term 'oily wastewater' comprises any wastewater containing an oil fraction, that could cover petroleum and its derivatives, but also fats, vegetable oils, and others [2]. Furthermore, oily wastewater may contain bio-refractory substances which hinder biological treatments [3]. The bio-refractory compounds can be dispersed in the oily and aqueous phases, according to their properties (lipophilic or hydrophilic character, solubility, or partition coefficient). Lipophilic pollutants usually found in oily effluents can be classified as aliphatic, aromatics, nitrogen-sulfur-oxygen-(NSO)-containing compounds, or asphaltenes [4,5]. Treating oily wastewater is challenging, especially when bio-refractory pollutants are present in the matrix [6].

Oily wastewaters are commonly subjected to physical and chemical

* Corresponding author at: Centro de Investigação de Montanha (CIMO), Instituto Politécnico de Bragança, Campus de Santa Apolónia, 5300-253 Bragança, Portugal.
E-mail address: htgomes@ipb.pt (H.T. Gomes).

https://doi.org/10.1016/j.cattod.2023.01.008
Received 26 November 2022; Received in revised form 3 January 2023; Accepted 11 January 2023
Available online 18 January 2023

processes, such as gravity separation, flocculation, and flotation, which are sufficient to remove free and dispersed oil (droplet size > 50 μm) [7,8]. After these conventional treatments, an oily sludge is usually formed, and further treated by pyrolysis, biological treatments, or combustion. However, these methods lead to the complete removal/degradation of high-added value oily compounds present in the sludge [9], and processes that result in the degradation of high-added value products imply in economic loss [3]. Thus, alternatives should be sought that allow the removal of hazardous lipophilic contaminants in oily wastewater, permitting the reuse of both the water and oily phases. Most works related to the treatment of oily wastewater focus on the full degradation of the oily fraction only [10–14]. However, advanced oxidation processes (AOPs) have also shown promising results in the selective removal of hazardous compounds from oily wastewater [3,15,16], simultaneously treating water and oily phases. Strategies based on the selective removal of hazardous compounds through oxidation processes are primarily studied to remove nitrogenated and sulfonated compounds from liquid fuels [17].

Among the AOPs, catalytic wet peroxide oxidation (CWPO) should be highlighted for being a low-cost process. CWPO relies on the selective decomposition of H_2O_2 into highly oxidizing radicals ($HO^{\bullet}$ and $HOO^{\bullet}$) through the action of proper catalysts [15]. Several catalysts have been studied in the abatement of a range of compounds using CWPO, such as compost-based [15] and clay-based [18,19] catalysts, activated carbons obtained from wastes [20], carbon nanotubes [3], among others. The characteristics of the catalyst play a relevant role in CWPO, including the surface chemistry, textural properties, adsorption ability towards the pollutant, among others. The relationship between catalyst properties and activity in CWPO has been well documented in the literature [21,22].

Carbon-based materials should be considered as interesting alternatives for this application due to the ease of manipulating their surface chemistry to display the desired properties [23,24]. One common approach to alter the surface properties of carbon-based materials is through the introduction of heteroatoms, known as doping [23]. Several atoms have been studied as dopants of carbon materials [23], emphasizing nitrogen, which can be inserted in the backbone structure of the carbon material due to its similar size to carbon atoms [23], producing metal-free materials with improved catalytic performances. N-doping has been shown to modify the characteristics of several carbon-based materials, improving their catalytic activity toward the degradation of contaminants by AOPs [25–27], and previous works have suggested that N-doping may be an interesting approach for CWPO [24,25,27], especially to treat oily wastewaters [3]. Carbon nanotubes (CNTs) synthesis *via* chemical vapor deposition (CVD) is a viable alternative for *in situ* N-doping, for instance, by using acetonitrile as simultaneous nitrogen and carbon source, leading to the growth of carbon-based structures with nitrogen heteroatoms interlayered in the backbone of the CNTs. The synthesis of CNTs with distinct undoped and N-doped sections, *i.e.* Janus-like CNTs, can be achieved by changing the precursor fed to the CVD reactor, as demonstrated in previous works [3,25,28]. Janus Particles (JPs) are materials that display spatially isolated distinct chemistries [29], such as undoped and doped sections. Due to the compartmentalization between the sides with different chemistries, JPs are expected to display a distinct behavior at liquid-liquid interfaces compared to homogeneous particles [30], and thus should provide an exciting platform for biphasic reactions.

This paper deals with the selective denitrification of a simulated contaminated oily wastewater containing 4-NP. CWPO reactions were conducted considering both aqueous-only and emulsified systems, where Janus-like CNTs acted both as catalysts and emulsion stabilizers. The role of nitrogenated species in the decomposition of H_2O_2 was correlated for both aqueous-only and emulsified reactions. Similarly, the influence of emulsion formation and the droplet sizes in the abatement of 4-NP and other parameters were correlated. While the role of the distinct nitrogenated species in the decomposition of H_2O_2 for CWPO in aqueous phase has been previously studied [31], to the best of our knowledge, no other paper has investigated the role of nitrogenated species in CWPO under emulsified systems, nor the synergistic relationship between the decomposition of H_2O_2 under an emulsified system and the droplet size of the emulsion.

2. Materials and methods

2.1. Reagents and materials

4-nitrophenol (4-NP, 98%) was obtained from Acros Organics. Hydrogen peroxide (H_2O_2, 30% w/v) and orthophosphoric acid (85%) were obtained from Fisher Chemical. Titanium (IV) oxysulfate (15 wt% in dilute sulfuric acid, H_2SO_4, metal basis 99.99%) was obtained from Sigma Aldrich. Sulfuric acid (98%) was obtained from Labkem. Sodium sulfite anhydrous (98%) was purchased from Panreac. 2,2,4-trimethylpentane (isooctane) and acetonitrile were obtained from VWR Chemicals. Unless when stated otherwise, distilled water was used all throughout the work. Acetonitrile (99.5%) used for synthesizing CNTs was obtained from Sigma-Aldrich, whereas the nitrogen, ethylene and hydrogen gases were obtained from Air Liquide. The precursors used to synthesize the catalyst for the growth of CNTs, namely aluminum nitrate nonahydrate (≥98%), iron (III) nitrate nonahydrate (≥98%), and ammonium hydroxide (≥98%, NH_3 basis) were obtained from Sigma-Aldrich, and cobalt (II) nitrate hexahydrate (≥98%) was supplied by Acros Organics.

2.2. Synthesis of CNT catalysts

The CNTs were synthesized by catalytic CVD in a fluidized-bed reactor using ethylene (as carbon source) and acetonitrile (as nitrogen and carbon source), as described elsewhere [3,25,28]. The carbon nanostructures were grown over an $AlCoFeO_4$ catalyst obtained using a citrate–nitrate gel combustion method by adapting a procedure reported elsewhere [32]. Appropriate amounts of Fe, Ni and Al salts were dissolved in water. The pH of the solution was adjusted to 6.5 – 7.0 [33] using ammonium hydroxide, and the resulting solution was placed in oven at 60 °C overnight. Once the gel was formed, the combustion and calcination steps were conducted in a muffle at 200 °C for 2 h and 400 °C for 5 h, respectively. The catalyst was reduced *in-situ* using H_2 (40 vol% in N_2) for 30 min at 650 °C, as described elsewhere [34], followed by the CVD growth of the CNTs at the same temperature. Ethylene (E) and acetonitrile (A) were fed to the system following 6 distinct approaches, leading to 6 different CNT materials, whilst maintaining the total feed time of 20 min. Both the total feed time and the individual feed times chosen for ethylene and acetonitrile were based on previous works [3,24,25,28]. The first sample of CNT was obtained by feeding ethylene for 20 min, leading to **E20**. Similarly, **A20** was obtained by feeding N_2/acetonitrile to the reactor for 20 min (N_2 was bubbled through acetonitrile at 35 °C). The Janus-like CNTs were obtained by feeding ethylene followed immediately by acetonitrile as follows: **E15A5** resulted from feeding 15 min of ethylene followed by 5 min of N_2/acetonitrile; **E10A10** resulted from 10 min of ethylene followed by 10 min of N_2/acetonitrile; **E5A15** was obtained after 5 min of ethylene and 15 min of N_2/acetonitrile; finally, **E1A19** was produced after feeding 1 min of ethylene followed by 19 min of N_2/acetonitrile. All samples were purified under reflux at 140 °C for 3 h using a H_2SO_4 50 vol% solution, and thoroughly washed with distilled water until neutrality of the rinsing waters. The resulting materials were dried in oven at 80 °C overnight.

2.3. Characterization of CNT catalysts

The textural properties were studied by using N_2 adsorption-desorption isotherms, obtained at 77 K in a Quantachrome NOVA-TOUCH XL4 apparatus. The specific surface area (S_{BET}) was calculated

by the BET method in the range of p/p^0 0.05 – 0.35. The external surface area (S_{ext}) was obtained by the *t*-method (thickness was calculated using ASTM standard D-6556–01). The total pore volume (V_{Total}) was determined at $p/p^0 = 0.98$. Calculations were done with TouchWinTM software v1.21. Thermogravimetric analysis (TGA) was performed in a NETZSCH STA 409 PC/PG apparatus in air atmosphere from 50 to 900 ºC at 10 °C min^{-1}. Ashes were determined as the remaining weight by the end of TGA. Elemental analysis was performed in a CHNS analyzer (Flash 2000, Thermo Fisher Scientific), equipped with a thermal conductivity detector. Fourier Transform Infrared (FT-IR) spectroscopy was conducted in a Perkin Elmer FT-IR spectrophotometer and recorded with a resolution of 4 cm^{-1} from 450 to 4000 cm^{-1} using a UATR accessory. X-ray photoelectron spectroscopy (XPS) spectra were acquired in a PHI-5701 equipment (Physical Electronics). Transmission electron microscopy (TEM) images were obtained in a JEOL 1011 apparatus operating at 100 kV. Fe and Co content in the CNTs were determined by atomic absorption (PinAAcle 900 T, Perkin Elmer) by digesting the ash of the samples with *aqua regia* (105 °C, 9 h).

2.4. Catalytic wet peroxide oxidation (CWPO) of 4-NP in aqueous medium

The aqueous phase experiments were carried out in a well-stirred (600 rpm) round flask reactor coupled with a condenser and a temperature controller. The reactor was loaded with 50 mL of 4-NP solution ($[4\text{-NP}]_0 = 1$ g L^{-1}), previously acidified to reach $pH_0 = 3.5$ (using a 0.5 M H_2SO_4 solution) and heated to 80 °C. The pH and temperature were chosen based on previous works [19,35–37]. Upon reaching the desired temperature, the stoichiometric amount of H_2O_2 needed for complete oxidation of 4-NP was added ($[H_2O_2]_0 = 3.6$ g L^{-1}). After complete mixing, the catalyst was added ($c_{cat} = 2.5$ g L^{-1}), setting this as instant $t_0 = 0$ min. Reaction samples were periodically withdrawn to determine the TOC and concentration of H_2O_2, 4-NP, and its intermediates. Moreover, the content of other aromatics (ARM), the pH of the reaction and leached Fe and Co were measured by the end of the reaction. The reactions were monitored for 24 h to allow for comparison with data previously obtained in the group [35–37].

2.5. Biphasic catalytic wet peroxide oxidation of 4-NP

2.5.1. Preparation of simulated oily wastewater containing 4-NP

The solution simulating a contaminated oily wastewater was prepared by dissolving 4-NP in 900 mL of ultrapure water acidified at pH of 3.5 by means of a 0.5 M H_2SO_4 solution. Then, 100 mL of 2,2,4-trimethylpentane was added to the flasks, and left resting for longer than a week in order to reach equilibrium between the concentration of 4-NP in oily and aqueous phases. The amount of 4-NP initially dissolved in water was calculated in order to reach 1 g L^{-1} of 4-NP concentration in the aqueous phase to ($[4\text{-NP}]_0^W = 1$ g L^{-1}), considering a partition coefficient of *log P* = - 2.09 (alkane-water mixtures [38]), leading to an expected concentration in the oily phase of $[4\text{-NP}]^\circ_{0,\ theoretical} = 8$ mg L^{-1} (experimental concentration was determined as $[4\text{-NP}]^\circ_0 = 10$ mg L^{-1}). The concentration of 4-NP in both oil and aqueous phases were regularly monitored during this work and prior to perform an assay. The volume of water and oil phases removed from the storage bottle were collected in such a way to always maintain the O/W volume ratio of 1:9.

2.5.2. Emulsion formation

Prior to conduct the reaction runs, the ability of the catalysts to form emulsions was assessed. Briefly, 4.5 mL of distilled water at pH of 3.5 and 0.5 mL of 2,2,4-trimethylpentane (O/W = 1:9 vol./vol.) were loaded in 10 mL flasks, followed by 12.5 mg of catalyst ($c_{cat} = 2.5$ g L^{-1}). The medium was sonicated for 10 min (Ultrasounds-H, JP-Selecta) and then observed in a Nikon Eclipse 50i microscope coupled to a Nikon digital sight DS-SM camera.

2.5.3. Reaction runs

The reactions were conducted considering the same operating conditions as reported for the aqueous phase reactions, *i.e.,* 80 °C, pH_0 of aqueous phase = 3.5, $c_{cat} = 2.5$ g L^{-1} (considering the whole volume of the system), $V_{total} = 50$ mL, $[4\text{-NP}]_0^W = 1$ g L^{-1}, and stoichiometric amount of H_2O_2 to completely oxidize 4-NP ($[H_2O_2]_0 = 3.6$ g L^{-1}), and an O/W ratio of 1:9 (volume basis). As described above, the reaction medium (oil + water phase) was heated to the desired temperature, and then H_2O_2 was added, followed by the catalyst, defining this moment as $t_0 = 0$ min. The reaction medium was sonicated for 10 min (Ultrasounds-H, JP-Selecta) to form the emulsion [3]. Samples were periodically withdrawn from the emulsion. Next, oily and aqueous phases were separated by centrifugation to monitor (i) the concentration of H_2O_2, 4-NP, its oxidized intermediates, and TOC in the aqueous phase; and (ii) 4-NP in the oily phase. Other aromatic compounds (ARM), pH of the reaction and leached Fe and Co were determined by the end of experiment. A non-catalytic run was also performed to assess the removal of the pollutant (the reaction medium was also submitted to sonication, as described above). Preliminary runs to investigate the possible oxidation of 2,2,4-trimethylpentane (used to prepare the oily effluent) were conducted by measuring the increase in TOC in the water phase in the absence of 4-NP, negligible oxidation being observed.

2.6. Analytical techniques

The total organic carbon (TOC) content of the aqueous phase was measured in a SHIMADZU TOC-L equipment. H_2O_2 concentration in the aqueous phase was determined by a colorimetric method described elsewhere [19]. 4-NP and its oxidized intermediates in the aqueous phase were determined by high performance liquid chromatography (HPLC) using a Jasco system equipped with a UV-Vis detector (UV-2075 Plus), a quaternary gradient pump (PU-2089 Plus) for solvent delivery (0.3 mL min^{-1}) and a NUCLEOSIL 5 μm C18–100 Å column (150 mm × 2.1 mm). The UV-Vis detector was set at a wavelength of 277 nm. The mobile phase consisted of a mixture of ultrapure water with phosphoric acid (0.15 wt%) (**A**) and acetonitrile (**B**), filtered with a membrane filter (0.45 μm). A non-isocratic mobile phase composition was used, as given in Fig. S1. Retention times and limits of detection and quantification for 4-NP, 4-nitrocatechol (4-NTC) and hydroquinone (HQ) are described in Table S1. 4-NP in the oily phase was determined *via* UV-Vis (T70 spectrometer, PG Instruments, Ltd.) at the wavelength of 284 nm. Other aromatic compounds (ARM) were determined by diluting aqueous samples in a buffer solution at pH = 7 and measuring their absorbance at 254 nm, using 4-NP as a reference substance. The pH was measured in a PHS-3BW Benchtop pH/mV/°C meter (Bante Instruments). Leached Fe and Co were measured using atomic absorption (PinAAcle 900 T, Perkin Elmer).

2.7. Calculation methods

The efficiency of H_2O_2 consumption was calculated according to Eq. (1), as reported elsewhere [39].

$$\eta_{H_2O_2} = \frac{X_{TOC_{t=24h}}}{X_{H_2O_{2t=24h}}} \times 100\% \quad (1)$$

where $X_{TOCt=24\,h}$ and $X_{H2O2t=24\,h}$ represent the conversions of TOC and H_2O_2, respectively, after 24 h of reaction.

For oxidation runs in biphasic media, conversion of 4-NP was reported according to Eq. (2).

$$X_{4-NP} = 1 - \frac{n_{4-NP^W_{t=i}} + n_{4-NP^O_{t=i}}}{n_{4-NP^W_{t=0}} + n_{4-NP^O_{t=0}}} \quad (2)$$

where $n_{4\text{-}NPt=i}^{W}$, $n_{4\text{-}NPt=i}^{O}$, $n_{4\text{-}NPt=0}^{W}$, and $n_{4\text{-}NPt=0}^{O}$ stand for the number of moles of 4-NP in aqueous phase at $t = i$, 4-NP in oily phase at $t = i$, 4-NP in aqueous phase at $t = 0$, and 4-NP in oily phase at $t = 0$, respectively,

and where *i* refers to the time after catalyst addition, and 0 to the time when the catalyst is added.

The TOC of unknown products ($TOC_{unknown\ products}$) was determined by subtracting the TOC experimentally measured ($TOC_{experimental}$) from the contribution to TOC of the compounds detected using HPLC (*i.e*, 4-NP, 4-NTC and HQ). The theoretical TOC due to 4-NP during the reaction was calculated by using data obtained from HPLC, according to Eq. (3), and the theoretical TOC of the oxidized intermediates, *viz.* 4-nitrocatechol (4-NTC) and hydroquinone (HQ), also obtained from HPLC data, was calculated according to Eqs. (4)–(5). The $TOC_{unknown\ products}$ was calculated according to Eq. (6).

$$TOC_{4-NP} = [4-NP]\cdot 0.517 \quad (3)$$

$$TOC_{4-NTC} = [4-NTC]\cdot 0.465 \quad (4)$$

$$TOC_{HQ} = [HQ]\cdot 0.654 \quad (5)$$

$$TOC_{unknownproducts} = TOC_{experimental} - TOC_{4-NP} - TOC_{4-NTC} - TOC_{HQ} \quad (6)$$

The limit of detection (LOD) and limit of quantification (LOQ) for the concentrations obtained with HPLC were respectively calculated according to Eqs. (7) and (8):

$$LOD = \frac{3.3\sigma}{slope} \quad (7)$$

$$LOQ = \frac{10\sigma}{slope} \quad (8)$$

where *"σ"* is the standard deviation of the response and *"slope"* refers to the slope obtained with the calibration curve.

3. Results and discussion

3.1. Characterization of CNT samples

The elemental composition of the synthesized CNTs is shown in Table 1. As it can be observed, the increase in time feeding of acetonitrile influences the nitrogen content of the CNTs. The CNTs synthesized with lower acetonitrile feeding (E20 and E15A5) resulted in low content of N (0% and 0.15%, respectively). The material E10A10 also resulted in low incorporation of N on its structure (0.20%). On the other hand, E5A15, E1A19 and A20 all resulted in a higher incorporation of N (1.40%, 1.83% and 1.79%, respectively). The feeding time and the expected N content on the CNTs can be well correlated by a linear regression (R^2 = 0.89, Fig. S2(a)). The values reported here regarding the N content of doped CNTs show some variance from those reported in the literature for materials obtained under similar conditions (CVD using acetonitrile as carbon/nitrogen source): 3.2–5.6% [3], 0.29–5.3% [25], 0.4–6.1% [28] and 1.9–5.0% [24] for partially doped CNTs synthesized at 650 °C over a Fe/γ-Al_2O_3 catalyst, and 2–9% [40] for partially doped CNTs synthesized at 600 °C over a red-mud-based catalyst for a total feeding of 30 min. Other papers also reported values of 2–6.4% for completely doped CNTs synthesized at 600–800 °C over a Mg-Co-Al catalyst for a total time of 3 h [41], 1.44–4.18% for completely doped CNTs at 700–850 °C over a Fe-Co/$CaCO_3$ catalyst for a total feeding time of 1 h [42]. The variance in N content observed in this work compared to previous works can be ascribed to the lower total feeding time (20 min), than in previous studies in which CVD was considered for at least 30 min

From the adsorption/desorption isotherms of the synthesized CNTs, shown in Fig. S3, we can observe low adsorbed N_2 volumes at a low relative pressure (p/p_0), as expected since CNTs are non-microporous materials. On the other hand, at higher relative pressures, a hysteresis loop between the adsorption and the desorption branches is observed. The textural properties of the materials, with S_{BET} varying from 180 to 240 $m^2\ g^{-1}$ and the total volume of pores from 0.97 to 2.27 $cm^3\ g^{-1}$ are summarized in Table 1. Those values are within the range reported in the literature [24,25,28,40]. As it can be observed, materials synthesized in the presence of acetonitrile display slightly higher surface area than materials synthesized with ethylene, likely due to the presence of defects in its structure increasing the external exposed surface. The volume of micropores determined by the *t-plot* method was found to be 0 for all materials. There is a positive correlation between incorporated N-content and S_{BET} (R^2 = 0.94, Fig. S2(b)).

Fig. 1 shows the TEM images of the Janus-like CNTs (E1A19, E5A15, E10A10, and E15A5), whereas TEM images of the CNTs prepared by single precursors, *i.e.*, ethylene and acetonitrile (E20 and A20, respectively) are already shown in our previous publication [3], where the only slight difference is that these materials are prepared by feeding the precursors during 30 min instead of 20 min. CNTs with irregular form and different dimensions (wall thickness and diameters) were successfully obtained over $AlCoFeO_4$ sequentially feeding ethylene and acetonitrile for different times. In the case of the materials synthesized with both precursors, it is possible to observe two distinct regions: one with more regular walls and smaller diameters, ascribed to the undoped section, and another region with a bamboo-like structure, ascribed to the nitrogenated section of the CNT. Those regions are highlighted in Fig. 1, considering a black and a red line for undoped and N-doped structures, respectively. Minimum external diameters in the range 9 – 14 nm were measured, primarily associated with the undoped sections, whereas maximum external diameters are in the range 21–27 nm, mostly ascribed to N-doped sections. Those agree with previous reports on the synthesis of undoped [3,43] and N-doped CNTs [3,25,44] considering ethylene and acetonitrile as carbon and carbon/nitrogen sources, respectively.

The XPS spectra and the relative atomic percentage content of the elements on the surface of each sample of CNT is displayed in Fig. S4. As it can be observed, increasing acetonitrile feed time in the synthesis of the CNTs increases the nitrogen content on the material's surface. In the materials synthesized with lower acetonitrile feed time (E15A5 and E10A10), the content of N on the surface (1.25% and 1.88%, respectively) is greater than the content of N in the bulk CNT (0.15% and 0.20%, respectively) as determined by CHNS analysis (Table 1). That suggests that the nitrogen seems to be primarily incorporated in the surface of the CNT rather than in the whole structure. On the other hand, the incorporation of oxygenated groups by acid washing does not seem to be affected by the nitrogen content, as the material that resulted in a higher incorporation of oxygenated species is E10A10 (9.19%), followed by E15A5, A20, E1A19, E5A15, and E20 (5.65%, 2.95%, 2.36%, 2.32%,

Table 1
Elemental composition and textural properties of the catalyst.

Sample	C (wt%)	N (wt%)	H (wt%)	S (wt%)	Ashes[a] (%)	Remaining[b] (%)	$S_{BET} = S_{ext}$ ($m^2 g^{-1}$)	V_{total} ($mm^3\ g^{-1}$)
A20	91.98 (± 0.41)	1.79 (± 0.10)	0.23 (± 0.00)	0.32 (± 0.07)	3.0	2.66	240	0.97
E1A19	92.91 (± 0.24)	1.83 (± 0.10)	0.25 (± 0.00)	0.20 (± 0.04)	2.9	1.89	230	2.27
E5A15	93.57 (± 0.28)	1.40 (± 0.06)	0.19 (± 0.01)	0.13 (± 0.02)	2.4	2.29	211	2.37
E10A10	93.92 (± 1.21)	0.20 (± 0.02)	0.20 (± 0.19)	0.61 (± 0.09)	1.6	3.45	187	2.24
E15A5	94.55 (± 0.10)	0.15 (± 0.00)	0.17 (± 0.06)	0.40 (± 0.02)	1.6	3.11	190	1.48
E20	97.62 (± 0.13)	0.00 (± 0.00)	0.12 (± 0.01)	0.07 (± 0.01)	0.3	1.87	180	2.17

[a] Obtained from TGA analysis.
[b] Calculated as 100-C-H-N-S-ashes.

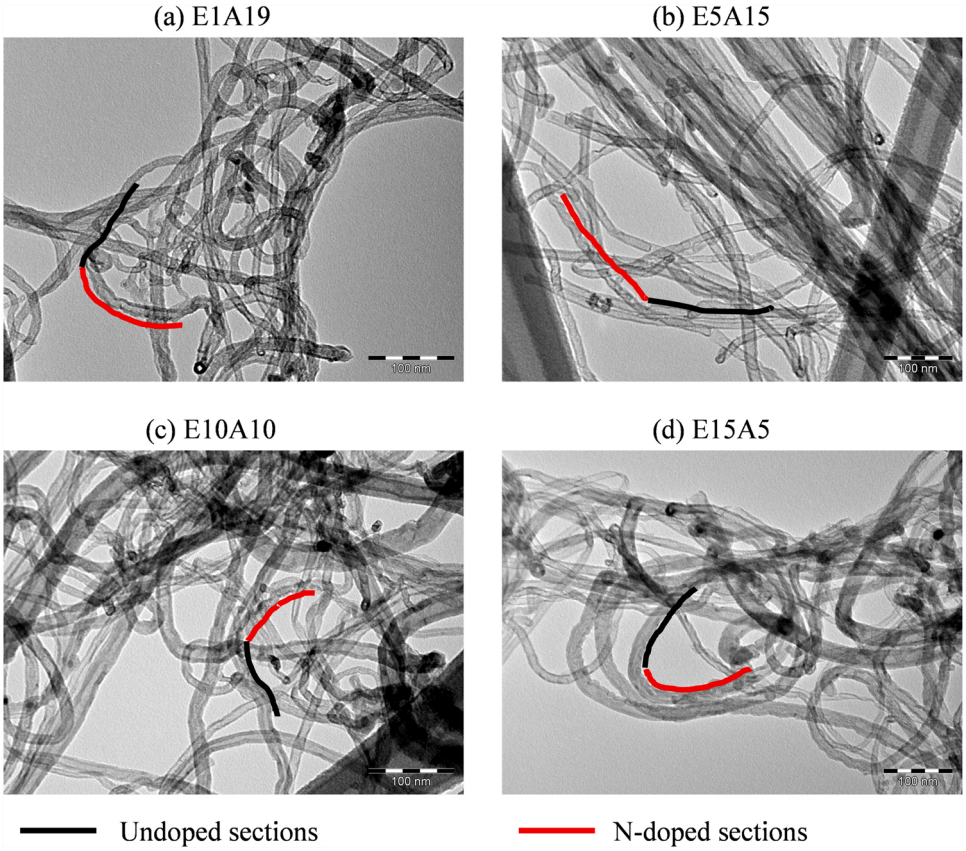

Fig. 1. TEM images highlighting some undoped (black line) and N-doped (red lines) sections of (a) E1A19, (b) E5A15, (c) E10A10 and (d) E15A5.

and 1.83%, respectively). Similarly, E10A10 and E15A5 also resulted in higher incorporation of sulfonated groups (2.31% and 1.21%, respectively).

Both O1s and N1s peaks were deconvoluted to assess the quantity of specific species that may influence the catalytic activities of the materials. The deconvolution curves for O1s region are displayed in Fig. S5 and N1s region is given in Fig. 2, and the atomic percentage of each group is described in Table S2. The binding energies used for deconvolution were chosen based on the literature [45]. The type of oxygenated groups introduced in the samples is very similar, regardless of the CNT, with carbonyl (531.1 eV), hydroxyl (532.3 eV) and C-O in esters and anhydrides groups (533.3 eV) representing 32–43%, 30–40% and 13–22% of the oxygenated groups present in the surface. Carboxylic groups (534.2 eV) are found in minimal quantities (<9%) in all materials particularly on E1A19 where only 0.03% of carboxylic groups were estimated. On the other hand, the type of nitrogenated groups introduced during synthesis clearly correlate with the feed time of acetonitrile. For the materials E15A5 and E10A10, which resulted in lower incorporations of N in the bulk structure of the CNTs, the main nitrogenated group introduced is quaternary N (401.4 eV), accounting for 86.35% and 94.56%, respectively. For the remaining materials, quaternary N was also introduced, corresponding to 33–45% of the nitrogenated content, closely followed by pyridinic N (398.7 eV), accounting for 36–39%. E1A19 and E5A15 also have significant fractions of pyridonic or pyrrolic N (400.3 eV), accounting for 19% and 16.5%, respectively. For E1A19 and A20, nitrogen oxides (402–405 eV), or nitrates, also account for an interesting fraction of the nitrogenated compounds (10–12%).

TGA (black lines, left Y axis) and DTG (blue lines, right Y axis) profiles are shown in Fig. 3, and the respective mass loss center and ashes content are shown in Table S3, together with a summary of the results of N-content, as determined by elemental analysis previously obtained (Table 1). There is a positive correlation between N-content and mass loss center (R^2 = 0.95, Fig. S2(c)) and ashes content (R^2 = 0.83, Fig. S2(d)). Upon decreasing nitrogen content on the CNT structure, the main center of mass loss generally shifts towards higher temperature levels (*i.e.*, 556, 558, 556, 638, 634 and 667 °C for A20, E1A19, E5A15, E10A10, E15A5, and E20, respectively). Similarly, a decrease in ashes content can be observed (3.0%, 2.9%, 2.4%, 1.6%, 1.6%, and 0.3% for A20, E1A19, E5A15, E10A10, E15A5, and E20, respectively). Thus, acetonitrile as a precursor generates CNTs that are less stable towards air oxidation compared to ethylene, as evidenced by the TGA and DTG profiles of A20 (Fig. 3(a)) and E20 (Fig. 3(f)), because mass losses are only observed above *ca.* 500 and 550 ºC, respectively. The difference of stability between the CNTs synthesized with acetonitrile or ethylene is related to the introduction of defects [25] or reactive centers [46] in the carbon structure due to N-doping, and to the presence of increasing amounts of residual catalyst in N-doped CNTs [47] as it has been shown that residual metallic particles in CNTs accelerate the decomposition of CNTs in air atmosphere [48]. TGA/DTG also allows to observe the formation of a single structure in each sample. A20 and E20 display only one mass loss peak, centered at 556 (Fig. 3(a)) and 667 °C (Fig. 3(f)), respectively. On the other hand, the materials prepared with both precursors display regions ascribed to two mass loss centers: one closer to 556 °C, ascribed to the N-doped sections, and one closer to 630 °C, ascribed to the undoped section. This is clearer in materials with higher incorporation of N, such as E1A19 (Fig. 3(b)) and E5A15 (Fig. 3(c)). Similar observations regarding the behavior towards the increase in temperature in oxidative atmospheres *vs*. doping are reported in the literature [3,25,28,40].

The content of Fe and Co, as determined by atomic absorption, is described in Table S3. The material A20 has the highest content of both Fe and Co (11 mg_{Fe} g_{cat}^{-1} and 14.8 mg_{Co} g_{cat}^{-1}), whereas E20 displays the lowest (0.9 mg_{Fe} g_{cat}^{-1} and 0.8 mg_{Co} g_{cat}^{-1}). The remaining materials

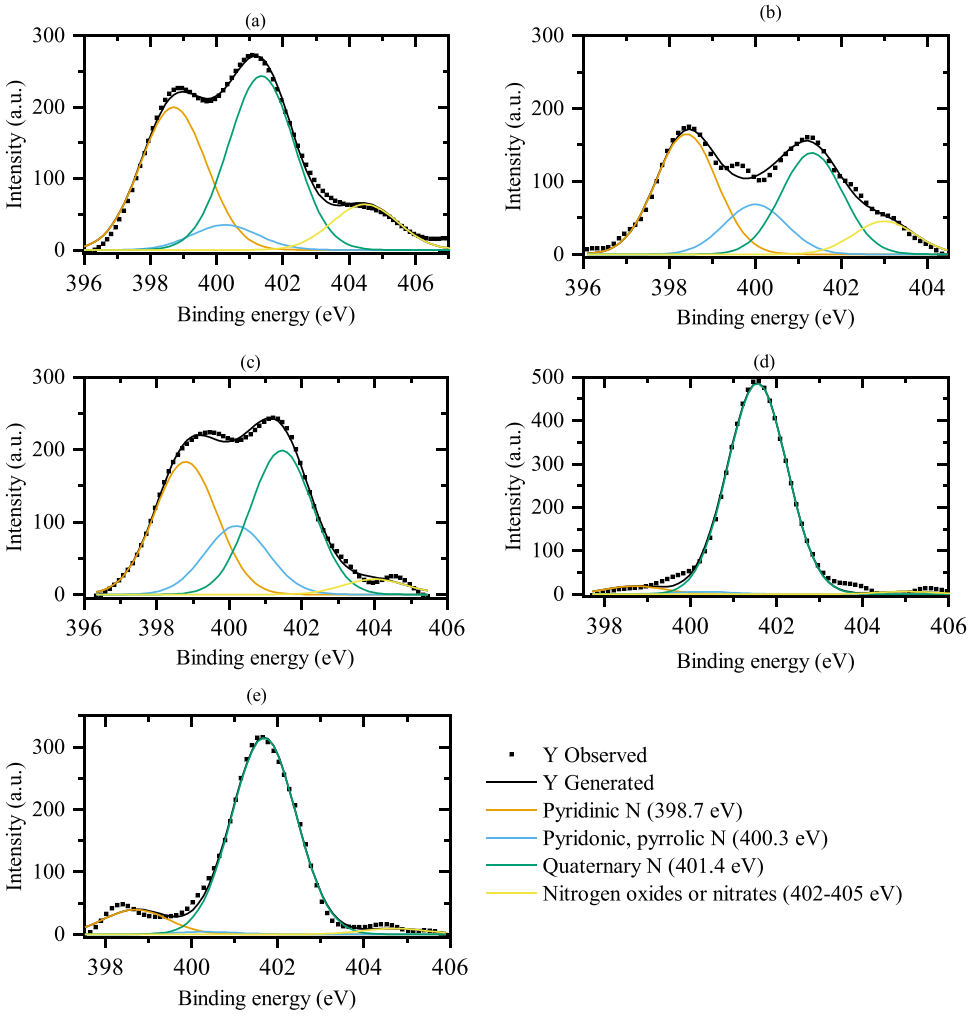

Fig. 2. N1s deconvolution for (a) A20, (b) E1A19, (c) E5A15, (d) E10A10, and (e) E15A5.

display intermediates contents of Fe (2.8 – 5.6 $mg_{Fe}\ g_{cat}^{-1}$) and Co (3.0 – 7.1 $mg_{Co}\ g_{cat}^{-1}$).

3.2. CWPO in aqueous medium

The results obtained in the CWPO of 4-NP conducted in water are presented in Fig. 4. As it can be observed, all tested CNTs are active catalysts, since the degradation of 4-NP and decomposition of H_2O_2 in 24 h ($37 < X_{4\text{-}NP} < 100\%$ and $40 < X_{H2O2} < 99\%$) are higher than those obtained in the non-catalytic run (23% of 4-NP was removed and 3% of H_2O_2 was decomposed in 24 h). The highest conversions of 4-NP (Fig. 4 (a)) were obtained in the presence of catalyst E10A10, closely followed by E15A5, with conversions reaching *ca.* 90% after 4 h of reaction. Specifically, followed by E20 with over 90% removal of 4-NP in 6 h of reaction. The reason ascribed to the higher conversion obtained with E20, E15A5 and E10A10 is due to the slow decomposition of H_2O_2 (4%, 28%, and 23%, respectively, after 1 h of reaction) compared to the three CNTs with higher N-content (A20, E1A19 and E5A15 led to 80% of H_2O_2 decomposition in 1 h of reaction). CNTs with a lower N-content (E20, E15A5 and E10A10) allow to slowly decompose H_2O_2 (> 80% conversion of hydrogen peroxide being achieved within 24 h of reaction). In fact, by taking a closer look at the overall conversion of H_2O_2 and 4-NP after 24 h of reaction, there is a clear trend regarding N-content and 4-NP and H_2O_2 conversions: a higher N-content results in faster H_2O_2 decomposition but fails to remove 4-NP properly (results are also summarized in Fig. S6). On the other hand, a lower N-content results in a more controlled decomposition of H_2O_2, leading to the complete removal of 4-NP.

A similar trend for TOC removal was observed. Materials with higher N-content resulted in lower TOC removal (19%, 22%, and 47% after 24 h of reaction for E5A15, E1A19 and A20, respectively) followed by E10A10 (48% TOC removal) and then the remaining materials with lower N-content (58% and 61% for E20 and E15A5, respectively).

The difference in the rates of decomposition of H_2O_2 in the presence of the catalysts with higher N-content (A20, E1A19 and E5A15) compared to those with catalysts with lower N-content (E15A5 and E10A10) can be associated to a series of factors. One of the factors is the different nitrogenated groups incorporated into the materials. Pyridinic N has been correlated with a faster decomposition of H_2O_2 [31] due to a stronger donating electron ability (strong Lewis basis) [49]. Similarly, graphitic N (or quaternary N) are considered weaker Lewis basis, and thus display lower ability to donate electrons [31], hindering the material's activity in the decomposition of H_2O_2. As can be observed in Table S2, the catalysts A20, E1A19 and E5A15 are rich in pyridinic N groups and poor in quaternary N (if compared to E5A15 and E10A10), thus explaining their higher activity towards H_2O_2 decomposition. The conversion of H_2O_2 *versus* the amount of pyridinic N can be well correlated by a linear regression with a $R^2 = 0.993$ (Fig. S2(e)), considering data obtained at 6 h of reaction. Furthermore, N-doped CNTs resulted in CNTs with a higher residue (Table S3), mostly comprised of iron, nickel and aluminum (resulting from the catalyst). Those metals are known to be active in Fenton processes. Hence,

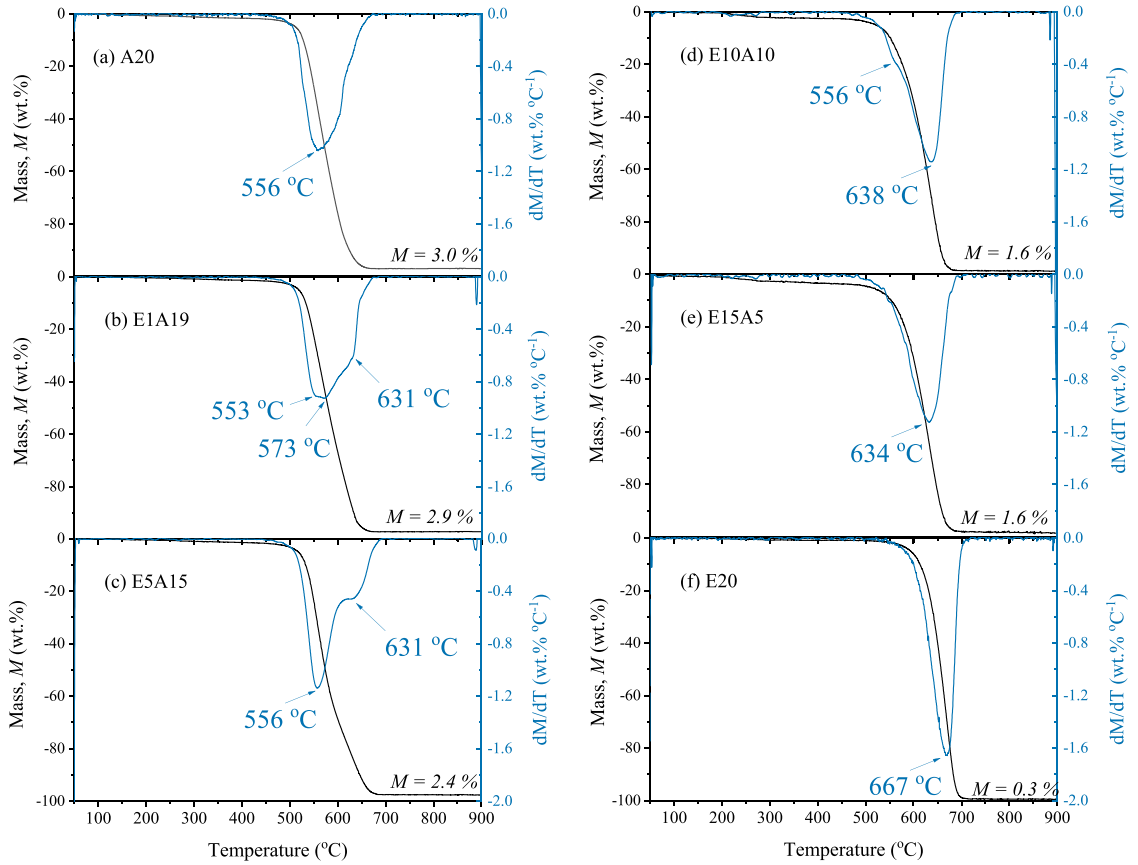

Fig. 3. TGA (black line, left Y axis) and DTG (blue line, right Y axis) profiles of (a) A20, (b) E1A19, (c) E5A15, (d) E10A10, (e) E15A5, and (f) E20 catalysts.

metallic residues within carbonaceous materials have been correlated to an increased activity in the decomposition of H_2O_2 [50]. However, despite having strong ability to decompose H_2O_2, poor removal of 4-NP and TOC in the presence of those materials was observed, resulting in low efficiency of H_2O_2 consumption ($\eta_{H2O2,}$ calculated accordingly to Eq. (1)). This efficiency for the materials with higher N-content was inferior (48%, 22%, and 19% for A20, E1A19 and E5A15, respectively) compared to materials with lower N-content (56%, 66% and 92% for E10A10, E15A5 and E20, respectively) (Fig. S6). The low efficiency obtained in the presence of materials with higher N-content was associated to parasitic reactions occurring due to the high rates of H_2O_2 decomposition [3], resulting into non-reactive species, such as H_2O and O_2 [51]. Furthermore, a proper interaction between the catalyst and the targeted pollutant is also crucial to increase likelihood of degradation as oxidation is expected to occur on the surface of the catalyst [52]. These results indicate that a fast decomposition of H_2O_2, as obtained in the presence of N-doped material, is not the main factor driving oxidation of 4-NP; likely indicating that other aspects of the operating conditions and catalysts, such as pH, adsorptive interactions between catalyst and pollutant, may play significant roles. In fact, the material prepared just with ethylene shows the highest H_2O_2 consumption efficiency (92%), likely due to its low affinity for H_2O_2 [24], allowing its controlled decomposition. This efficiency is considerably higher than those obtained by Fenton process [53].

Similar results were reported in the literature regarding the influence of N-doping, and the consequence in the pollutant removal and H_2O_2 decomposition. Martin-Martinez et al. (2016) reported that increasing N-content in CNTs resulted in higher H_2O_2 decomposition but poorer 4-NP and TOC removals [25]. In the work of Diaz de Tuesta et al. (2020) work, higher N-content also resulted in lower removal of 2-nitrophenol and TOC while resulting in high H_2O_2 conversions [3]. The overall results reported here regarding removal of 4-NP, TOC and efficiency of H_2O_2 consumption are comparable with other reports in the literature, as shown in Table 2.

Adsorption runs were conducted under the same operation conditions as CWPO runs, except for the absence of H_2O_2, to observe the adsorption contribution in the removal of 4-NP in the previous experiments. Fig. 5 gives the results obtained for 4-NP removal on each CNT after 24 h of contact time in comparison with the results obtained in CWPO after 24 h of reaction. Adsorption accounts for 14 – 25% of 4-NP removal after 24 h of contact time. On the other hand, higher removals of 4-NP were obtained in 1 h of CWPO (23–40% in 1 h of reaction (Fig. 4 (b)), and removals in the range 55–100% were observed after 24 h of reaction (Fig. 5); thus, oxidation is much more relevant than adsorption.

Fig. 6 shows the detected concentration of oxidized intermediates 4-nitrocatechol (4-NTC) and hydroquinone (HQ). For the first 2 h of reaction, the 4-NTC concentration increases for all CNTs tested (Fig. 6(a)). As expected E20, E10A10 and E15A5 are the most active materials, able to degrade this oxidized intermediate into other by-products (not detected), *i.e.*, the concentration of 4-NTC decreases after 2 h of reaction. In the presence of E5A15, E1A19 and A20, 4-NTC is not completely removed after 24 h of reaction, achieving concentrations of 56, 45, and 60 mg L^{-1}, respectively. The concentration of formed hydroquinone (HQ) upon time of reaction is depicted in Fig. 6(b). Similarly, E20, E15A5, and E10A10 reveal a higher performance in completely degrading this oxidated intermediate, achieving complete removal of HQ in 8, 4, and 8 h of reaction, respectively. E5A15 resulted in complete removal of HQ in 24 h, whereas E1A19 and A20 resulted in final concentrations of HQ of ~5 and 23 mg L^{-1}, respectively. Again, the distinct behavior towards the removal of the intermediates 4-NTC and HQ can be ascribed to the ability of the CNTs with lower N-content to control the decomposition of H_2O_2. Fig. S7 and Text S1 displays a brief explanation of the expected mechanism of degradation of 4-NP. A more detailed reaction mechanism for the oxidation of 4-NP in the presence of

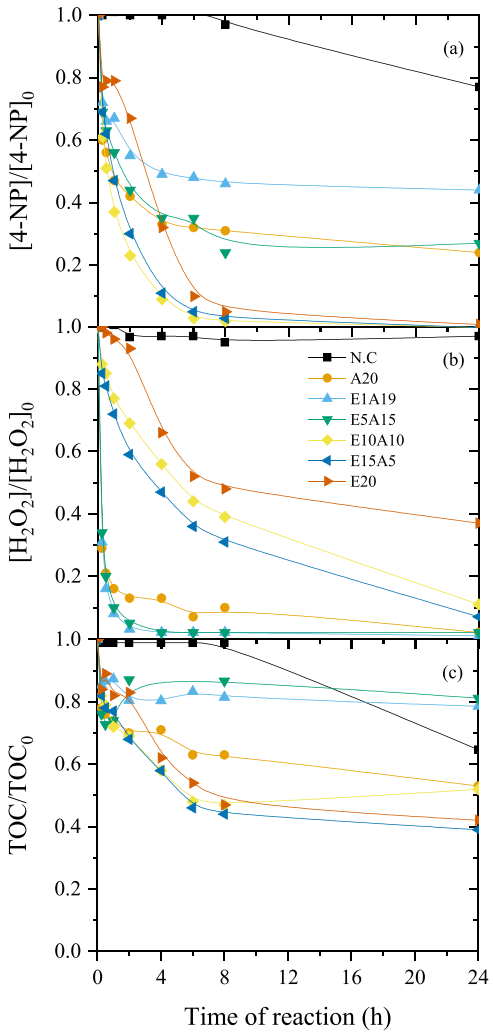

Fig. 4. Normalized concentration of (a) 4-NP, (b) H_2O_2, and (c) TOC along time of reaction, under the operational conditions: $[4\text{-NP}]_0 = 1\ g\ L^{-1}$, $[H_2O_2]_0 = 3.6\ g\ L^{-1}$, $c_{cat} = 2.5\ g\ L^{-1}$, $pH_0 = 3.5$, and $T = 80$ °C (N.C.= non catalytic run).

heterogeneous catalysts was proposed elsewhere [54–56]. The CNTs that resulted in complete degradation of 4-NP and its oxidized intermediates (E20, E10A10, E15A5) also resulted in an effluent with reduced coloration (Fig. S8) compared to CNTs that resulted in accumulation of either 4-NP, 4-NTC or HQ (A20, E1A19, E5A15). Color change along oxidation reactions have been previously reported for nitrophenols [57], and the observed color is highly associated with the level of oxidation reached [58].

The TOC profile free of the contribution from 4-NP and the quantified oxidized intermediates (Fig. S9) reaches its maximum at around 4 h of reaction in the presence of A20, E15A5 and E10A10, at 6 h of reaction in the presence of E5A15, and at 8 h of reaction in the presence of E20, and then it slightly decreases, evidencing that some of the intermediates not detected in this work are still further oxidized during the CWPO of 4-NP. In the presence of E1A19, the TOC free of 4-NP, 4-NTC and HQ reaches its maximum at 24 h of reaction, which may indicate that no further oxidation happens in the presence of these catalyst. By the end of reaction, other aromatic compounds (ARM) not detected by HPLC were still observed (Fig. S10). Lowest ARM concentrations (143, 44 and 44 $mg_{4\text{-NPeq.}}\ L^{-1}$ for E20, E15A5 and E10A10, respectively) were detected for CNTs with lower N-content. On the other hand, materials E5A15, E1A19 and A20 led to the formation of 483, 215, and 406 $mg_{4\text{-NPeq.}}\ L^{-1}$ of ARM, which cannot be explained by the 4-NP concentration detected in the end of reaction nor by the concentrations of 4-NTC or HQ (Fig. S10).

Furthermore, the pH was measured after 24 h of CWPO, reaching values of 2.42, 2.34, 2.31, 2.65, 2.42 and 2.60 with E20, E15A5, E10A10, E5A15, E1A19 and A20, respectively. The lowest pHs (2.34 and 2.31, from E15A5 and E10A10, respectively) by the end of the reaction runs were obtained in the presence of the materials that resulted in faster abatement of 4-NP, TOC, oxidized intermediates, and ARM concentration. Thus, this was ascribed to the formation of low-molecular weight carboxylic acid compounds (*e.g.*, oxalic, malic, acetic, formic, malonic,

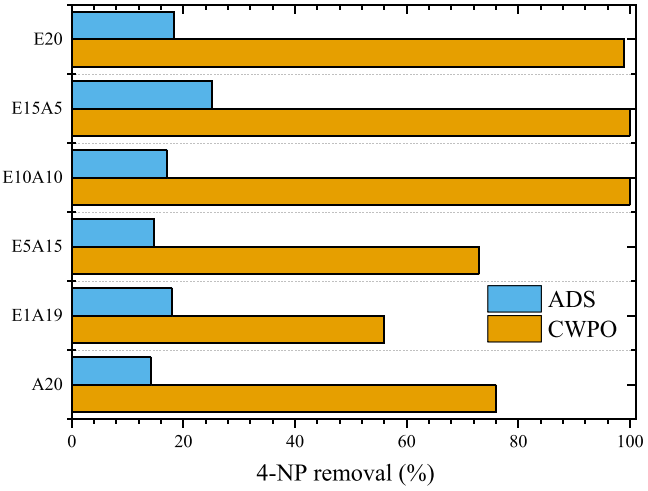

Fig. 5. Comparison between removal of 4-NP after 24 h of adsorption and CWPO under the operational conditions:: $[4\text{-NP}]_0 = 1\ g\ L^{-1}$, $[H_2O_2]_0 = 3.6\ g\ L^{-1}$ (CWPO only), $c_{cat} = 2.5\ g\ L^{-1}$, $pH_0 = 3.5$, and $T = 80$ °C.

Table 2
Comparison with reported removals of 4-NP and TOC, and efficiency of hydrogen peroxide consumption (η_{H2O2}) for the aqueous phase CWPO of 4-NP with carbon-based materials.

Catalyst	Conditions					Results			Ref.
	$[4\text{-NP}]_0\ (g\ L^{-1})$	pH	T (°C)	$c_{cat}\ (g\ L^{-1})$	$[H_2O_2]_0\ (g\ L^{-1})$	$X_{4\text{-NP}}$ (%)	X_{TOC} (%)	η_{H2O2} (%)	
rGO	5	3	50	2.5	17.8 (stoic.)	~25–65%	~23–25%	~45–75%	[39]
N-CNT	5	3	50	2.5	17.8 (stoic.)	9–100%	2–59%	2–100%	[24]
Lignin-based AC	5	3	50	2.5	17.8 (stoic.)	~17–65%	~18–20%	~30–100%	[64]
$CoFe_2O_4$/MGNC	5	3	80	2.5	17.8 (stoic.)	100%	55%	77%	[37]
Carbon black	5	3	80	2.5	17.8 (stoic.)	95–100%	N.M.	N.M.	[35]
AC	5	3	80	2.5	17.8 (stoic.)	23–32%	14–32%	31–91%	[36]
CX/CoFe	5	3	50	2.5	17.8 (stoic.)	98.5%	67%	84%	[65]
N-CNT	5	3	50	2.5	17.8 (stoic.)	10–100%	18–60%	20–100%	[25]
Compost-based	5	3	50	2.5	17.8 (stoic.)	75–100%	N.M.	N.M.	[15]
N-CNT	1	3.5	80	2.5	3.6 (stoic.)	37–100%	19–61%	19–92%	This study

AC = Activated carbon. XG = xerogel. Stoic. = stoichiometric.

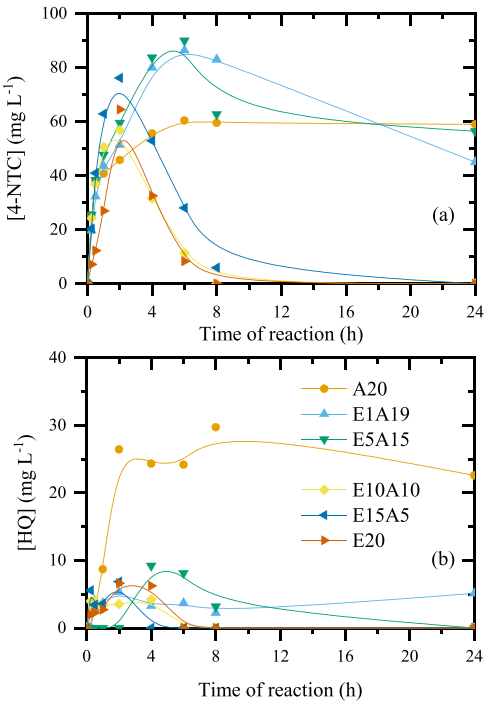

Fig. 6. Detected concentration of (a) 4-nitrocatechol (4-NTC) and (b) hydroquinone (HQ) along the reaction under operational conditions: $[4\text{-NP}]_0 = 1$ g L^{-1}, $[H_2O_2]_0 = 3.6$ g L^{-1}, $c_{cat} = 2.5$ g L^{-1}, $pH_0 = 3.5$, and T = 80 °C.

and maleic) during the CWPO of 4-NP, as observed in previous works [25,35]. Other works have also reported a decrease in pH after CWPO of other pollutants for highly performing catalysts [19]. The CNTs with highest performance in terms of removal of the pollutant, its intermediates and TOC (E15A5 and E10A10) resulted in the lowest pH (2.34 and 2.31, respectively) by the end of the reaction. Minor leaching of Fe and Co (< 2.0 mg L^{-1}) were detected.

3.3. CWPO in a biphasic medium

Before the CWPO experiments in biphasic medium, the ability of the CNTs to act as stabilizers in emulsion was assessed considering equivalent conditions to those used for oxidation experiments in biphasic system (O/W = 1:9 vol./vol. and 12.5 mg of the catalyst, *i.e.*, c_{cat} = 2.5 g L^{-1}). Most materials (E20, E10A10, E5A15, E1A19 and A20) allowed the formation of emulsions under the studied conditions (as shown in Figs. S11 and 7). The use of E15A5 resulted in a very poorly stabilized emulsion, even breaking before it was possible to collect a sample for analysis. In the presence of the materials synthesized with single precursors (E20 and A20, Fig. S11), the emulsions formed were poorly stable, and broke within 30 min upon formation. In fact, the coalescence of the oily droplets in the presence of E20 (Fig. S11(b)) can be easily observed. The materials with the Janus structure allowed to form emulsions with higher stability (Fig. 7). Emulsions were stable for 30–240 min depending on the material, and E1A19 resulted in the most stable emulsion (up to 4 h without stirring). The droplet size also depends greatly on the material acting as emulsifier: E1A19 resulted in the lowest average droplet size and with a more homogeneous distribution of droplets (1.02 ± 0.22 μm) followed by E5A15 (2.64 ± 1.17 μm) and E10A10 (2.74 ± 1.29 μm).

Hence, the CNTs were tested on the selective oxidation of 4-NP under a biphasic system (O:W = 1:9 vol./vol.), simulating a contaminated oily wastewater. Fig. 8 gives the results obtained for the reactions conducted under a biphasic system. E1A19 shows the highest catalytic activity, with a 97% removal of 4-NP being achieved after 4 h of reaction (Fig. 8 (a)). Similarly, E1A19 also resulted in the fastest consumption of H_2O_2, leading to > 90% decomposition in 8 h of reaction (Fig. 8(b)). The remaining materials behaved similarly in the oxidation of 4-NP and allowed a removal of 4-NP > 98% in 24 h of reaction, demonstrating to be active catalysts. The activity towards H_2O_2 decomposition follows the order E1A19 > A20 > E5A15 > E10A10 ~ E15A5 > E20 (Fig. 8(b)). E1A19 was again the material that led to obtain the highest removal of TOC in biphasic oxidation reactions (Fig. 8(c)), with 50% TOC abatement. The least performing material was E5A15, with 23% of TOC abatement. The remaining materials led to TOC removals in the range 30 – 40%. High performing materials also resulted in reduction in the color of the oily effluent compared to poor performing materials (Fig. S12).

4-NTC was also detected in the aqueous phase during biphasic oxidation. The results are shown in Fig. 9. In the presence of E1A19, 4-NTC is rapidly formed and decomposed. It reaches its peak in less than 2 h of reaction (*ca.* 110 mg L^{-1}) and is no longer detected in 8 h of reaction. In the presence of the remaining materials, of the Janus-like materials (E10A10, E5A15 and E15A5), 4-NTC is completely removed by 24 h of reaction. On the other hand, in the presence of E20 and A20, 4-NTC is not completely oxidized, ending the reaction with 15 and 6 mg L^{-1} of 4-NTC, respectively.

As observed for the CWPO reactions conducted in aqueous solution, the reactivity toward H_2O_2 is governed by the different amounts of nitrogenated groups in the CNT samples, and the conversion of H_2O_2 can be well correlated to the content of pyridinic N, with a $R^2 = 0.964$ (Fig. S2(f)) considering data obtained at 24 h of reaction. In these experiments, the fast rates of H_2O_2 decomposition, due to pyridinic N, did not translate into higher rates of 4-NP removal or TOC abatement. In fact, the opposite was observed: increasing N content led to faster decomposition of H_2O_2, but also to lower removals of pollutant and TOC, being ascribed to side reactions leading to unreactive species [24]. On the other hand, in the runs conducted under biphasic system, the fast rate of H_2O_2 decomposition observed in the presence of E1A19 was translated into a faster removal of 4-NP and abatement of TOC, when compared to the remaining catalysts tested in the biphasic system, and when also compared to the performance of the same material in the aqueous phase runs. The performance of E1A19 in the biphasic system is associated with its ability to form emulsions with smaller droplets sizes (as discussed above and observed in Fig. 7), allied to its ability to maintain the emulsion for a longer period of time. The formation of smaller droplet sizes results in a higher contact between the oily and water phases, accelerating the mass transfer between the phases and promoting higher interaction between oxidant and pollutant. Similar results have been previously reported [3]. Furthermore, the droplets formed by E1A19 seem to be more disperse in the continuous phase (water) which may bear an influence on the experienced cage effect. The cage effect refers to an increased reaction probability between two encaged species. In the presence of E1A19 in biphasic system, due to the formation of well-dispersed small droplets of oil, a stronger cage effect may be experienced, entrapping $HO^{\bullet}$ radicals and 4-NP within the same cage, increasing the time window in which the two reactants remain close together and thus their interaction for reaction [59]. Increased conversion due to increased cage effect has been previously reported for emulsified systems [60–63]. Therefore, in oxidation runs under biphasic systems, emulsion formation allied to a high content of pyridinic N in carbon-based materials, may be the key towards faster and higher conversions of pollutant, oxidized intermediates and TOC.

The TOC profile free of the contribution of 4-NP and 4-NTC for the best-performing catalyst (E1A19) in biphasic system (Fig. S13) reaches its maximum at 8 h of reaction, and then slightly decreases at 24 h of reaction, pointing out that the non-identified intermediates still undergo oxidation. For the remaining CNTs, the TOC free of 4-NP and 4-NTC reaches a peak only after 24 h of reaction (Fig. S13). E1A19 also resulted a in low concentration of other aromatic compounds (52 $mg_{4\text{-NPeq.}}$ L^{-1}), as displayed in Fig. S14, whereas the remaining catalysts resulted in final concentrations of ARM of 369, 621, 249, 126, and 455 $mg_{4\text{-NPeq.}}$ L^{-1} for A20, E5A15, E10A10, E15A5, and E20, respectively. The pH of

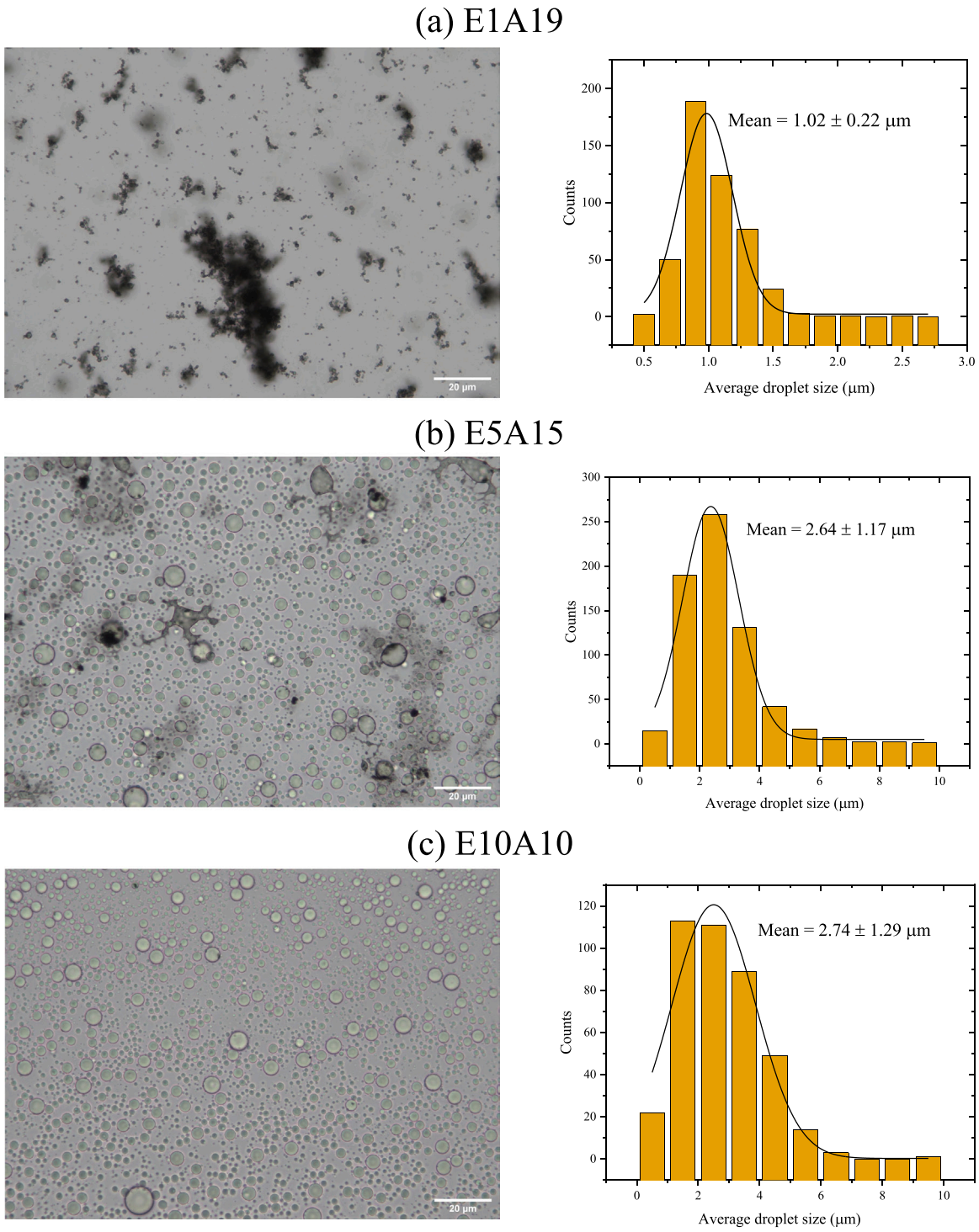

Fig. 7. Emulsion formation in the presence of (a) E1A19, (b) E5A15, and (c) E10A10. To the left, microscopic images (scale bar of 20 µm) and to the right histogram of the droplet sizes. (operational conditions: c_{cat} = 2.5 g L^{-1}, pH_0 = 3.5, O/W = 1:9 vol./vol., 10 min of ultrasound).

the aqueous phase by the end of the reaction decreased to 2.57, 2.42, 2.38, 2.45, 2.57, and 2.44 for E20, E15A5, E10A10, E5A15, E1A19 and A20, respectively, indicating the formation of carboxylic acids not detected by HPLC. By the end of the reaction, the removal of 4-NP from the oily phase reached values of 16%, 66%, 50%, 60%, 71% and 45% for E20, E15A5, E10A10, E5A15, E1A19 and A20, respectively. Observed leaching of Fe and Co were similar to reactions conducted under aqueous phase.

4. Conclusions

Janus-like CNTs containing defined undoped and N-doped sections were successfully synthesized by sequentially feeding ethylene and acetonitrile in a fluidized-bed reactor with only 20 min of total feeding time, as evidenced by TEM and TGA. By varying the time feeding of acetonitrile and ethylene, different amounts of nitrogen were incorporated into the structures, both in the bulk structure of the CNT as well as in its available surface. The proposed methodology also allows a good control over the type of nitrogenated compounds incorporated on the

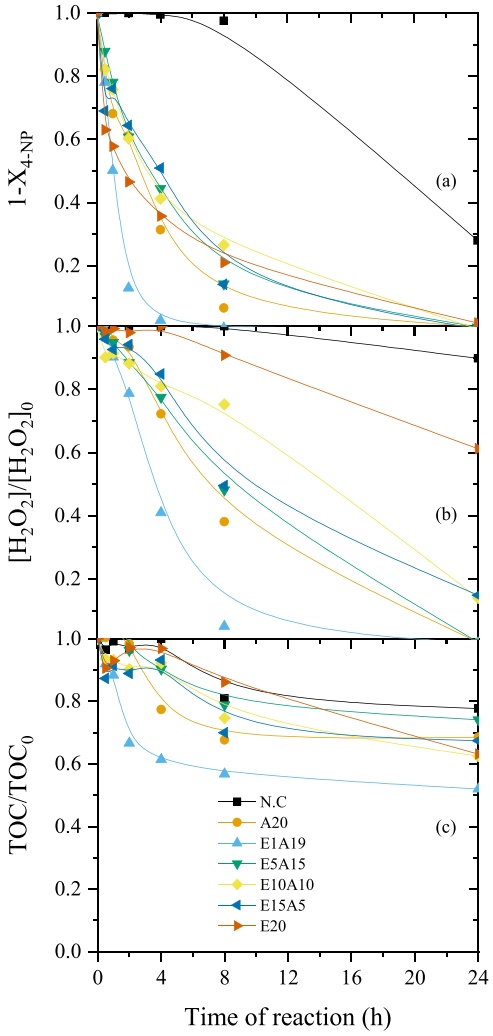

Fig. 8. Remaining (a) 4-NP (in both oily and aqueous phase) in the reaction medium and normalized concentration of (b) H_2O_2, and (c) TOC along time of reaction, under the operational conditions: $[4\text{-NP}]_0^W = 1$ g L^{-1}, $[H_2O_2]_0 = 3.6$ g L^{-1}, $c_{cat} = 2.5$ g L^{-1}, $pH_0 = 3.5$, T = 80 °C, O/W = 1:9 vol./vol., and 10 min of sonication. (N.C.= non catalytic run).

surface.

The synthesized Janus-like CNTs were tested in the CWPO of 4-NP under aqueous and biphasic systems by simulating the treatment of contaminated oily wastewater. CNTs with both N-doped and undoped arrangements in their structure are the materials that revealed the highest catalytic activity towards the degradation of the pollutant and its oxidized intermediates, TOC removal, and aromatics abatement, both in aqueous and biphasic medium. Especially, E10A10 and E5A15 have shown interesting behavior in aqueous experiments, resulting in the complete removal of 4-NP and detected oxidized intermediates, in a low value of other aromatic compounds and TOC, and good efficiency of oxidant consumption. The rate of H_2O_2 decomposition has been correlated to the content of pyridinic N on the surface of the material, independently of the reaction system (aqueous or biphasic). However, the efficiency of oxidant consumption depends greatly on the system: for aqueous phase reactions, faster rates result in parasitic reactions, hindering the abatement of 4-NP and TOC. On the other hand, in biphasic experiments, other factors play an important role, such as the formation of the emulsion and cage-like effects, and thus a faster rate of H_2O_2 decomposition resulted in higher removal of 4-NP and TOC. Thus, for reactions conducted in a biphasic medium, E1A19 is highlighted due to its higher abatement of TOC and faster removal of 4-NP, ascribed to its

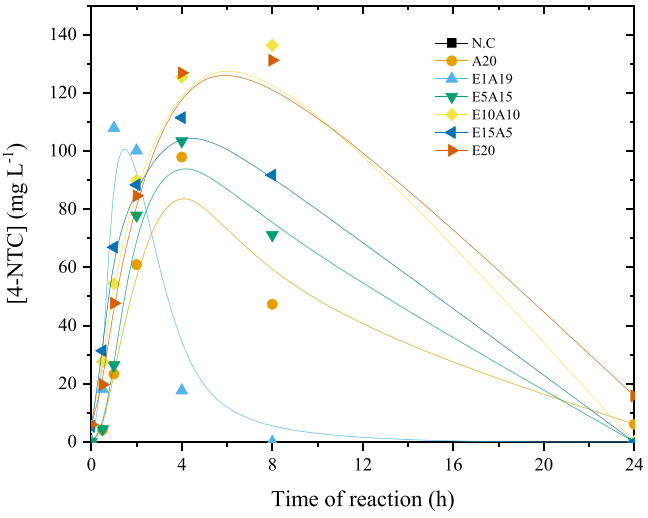

Fig. 9. Detected concentration of 4-nitrocatechol (4-NTC) along the reaction under operational conditions: $[4\text{-NP}]_0^W = 1$ g L^{-1}, $[H_2O_2]_0 = 3.6$ g L^{-1}, $c_{cat} = 2.5$ g L^{-1}, $pH_0 = 3.5$, T = 80 °C, O/W = 1:9 vol./vol., and 10 min of sonication.

ability to form emulsions with smaller and well-dispersed droplets. It is also the material that resulted in the highest pollutant removal from the oily phase.

Correlations between the physicochemical characteristics of the materials with the N-content demonstrate that the method used for the synthesis is powerful in designing materials with desired characteristics. Aligned with the controlled synthesis, this work also proved the link between N-content and efficiency in removing 4-NP by CWPO, already observed by previous authors in similar systems. This opens breaches to study more complex matrices closer to real scenarios, using materials prepared by the method presented here and designed to have lower N-content in their structure.

CRediT authorship contribution statement

Fernanda F. Roman: Investigation, Formal analysis, Writing – original draft. **Jose L. Diaz de Tuesta**: Writing – original draft, Conceptualization, Funding acquisition, Supervision. **Flávia K. K. Sanches:** Investigation, Formal analysis. **Adriano S. Silva**: Formal analysis, Writing – original draft. **Pricila Marin**: Supervision, Writing – review & editing. **Bruno F. Machado**: Investigation, Resources. **Philip Serp:** Supervision, Resources. **Marta Pedrosa:** Investigation, Writing – review & editing. **Adrián M. T. Silva**: Writing – review & editing, Supervision. **Joaquim L. Faria**: Writing – review & editing, Supervision. **Helder T. Gomes**: Funding acquisition, Project administration, Writing – review & editing, Supervision.

Declaration of Competing Interest

The authors declare that they have no known competing financial interests or personal relationships that could have appeared to influence the work reported in this paper.

Data availability

The data that has been used is confidential.

Acknowledgments

This work was financially supported by LA/P/0045/2020 (ALiCE), UIDB/50020/2020 and UIDP/50020/2020 (LSRE-LCM) funded by national funds through FCT/MCTES (PIDDAC); project

"PLASTIC_TO_FUEL&MAT – Upcycling Waste Plastics into Fuel and Carbon Nanomaterials" (PTDC/EQU-EQU/31439/2017), CIMO (UIDB/00690/2020), and project "Healthy Waters" (NORTE-01–0145-FEDER-000069) through FEDER under Program PT2020. Fernanda F. Roman acknowledges the Foundation for Science and Technology (FCT) and the European Social Fund (FSE) for the individual research grant with reference SFRH/BD/143224/2019. Adriano S. Silva was supported by the doctoral Grant SFRH/BD/151346/2021 financed by FCT with funds from NORTE2020, under MIT Portugal Program. Jose L. Diaz De Tuesta acknowledges the financial support through the program of Atracción al Talento of Comunidad de Madrid (Spain) for the individual research grant 2020-T2/AMB-19836.

Appendix A. Supporting information

Supplementary data associated with this article can be found in the online version at doi:10.1016/j.cattod.2023.01.008.

References

[1] L. Hui, W. Yan, W. Juan, L. Zhongming, A review: recent advances in oily wastewater treatment, Recent Innov. Chem. Eng. 7 (2015) 17–24.
[2] S. Jamaly, A. Giwa, S.W. Hasan, Recent improvements in oily wastewater treatment: Progress, challenges, and future opportunities, J. Environ. Sci. 37 (2015) 15–30.
[3] J.L. Diaz de Tuesta, B.F. Machado, P. Serp, A.M.T. Silva, J.L. Faria, H.T. Gomes, Janus amphiphilic carbon nanotubes as Pickering interfacial catalysts for the treatment of oily wastewater by selective oxidation with hydrogen peroxide, Catal. Today 356 (2020) 205–215.
[4] B. Mrayyan, M.N. Battikhi, Biodegradation of total organic carbons (TOC) in Jordanian petroleum sludge, J. Hazard Mater. 120 (2005) 127–134.
[5] M.V. Reddy, M.P. Devi, K. Chandrasekhar, R.K. Goud, S.V. Mohan, Aerobic remediation of petroleum sludge through soil supplementation: Microbial community analysis, J. Hazard. Mater. 197 (2011) 80–87.
[6] L. Yu, M. Han, F. He, A review of treating oily wastewater, Arab. J. Chem. 10 (2017) S1913–S1922.
[7] S. Varjani, R. Joshi, V.K. Srivastava, H.H. Ngo, W. Guo, Treatment of wastewater from petroleum industry: current practices and perspectives, Environ. Sci. Pollut. Res Int 27 (2020) 27172–27180.
[8] P. Kundu, I.M. Mishra, Treatment and reclamation of hydrocarbon-bearing oily wastewater as a hazardous pollutant by different processes and technologies: a state-of-the-art review, Rev. Chem. Eng. 35 (2018) 73–108.
[9] L.J. da Silva, F.C. Alves, F.P. de Franca, A review of the technological solutions for the treatment of oily sludges from petroleum refineries, Waste Manag Res 30 (2012) 1016–1030.
[10] D. Ma, H. Yi, C. Lai, X. Liu, X. Huo, Z. An, L. Li, Y. Fu, B. Li, M. Zhang, L. Qin, S. Liu, L. Yang, Critical review of advanced oxidation processes in organic wastewater treatment, Chemosphere 275 (2021), 130104.
[11] F. Görmez, Ö. Görmez, E. Yabalak, B. Gözmen, Application of the central composite design to mineralization of olive mill wastewater by the electro/FeII/persulfate oxidation method, SN Appl. Sci. 2 (2020) 178.
[12] Y. Mokhbi, M. Korichi, Z. Akchiche, Combined photocatalytic and Fenton oxidation for oily wastewater treatment, Appl. Water Sci. 9 (2019) 35.
[13] Y. Huang, M. Luo, Z. Xu, D. Zhang, L. Li, Catalytic ozonation of organic contaminants in petrochemical wastewater with iron-nickel foam as catalyst, Sep. Purif. Technol. 211 (2019) 269–278.
[14] J. Lee, W.-C. Cho, K.-M. Poo, S. Choi, T.-N. Kim, E.-B. Son, Y.-J. Choi, Y.M. Kim, K.-J. Chae, Refractory oil wastewater treatment by dissolved air flotation, electrochemical advanced oxidation process, and magnetic biochar integrated system, J. Water Process. Eng. 36 (2020), 101358.
[15] J.L. Diaz de Tuesta, G.F. Pantuzza, A.M.T. Silva, P. Praça, J.L. Faria, H.T. Gomes, Catalysts Prepared with Matured Compost Derived from Mechanical-Biological Treatment Plants for the Wet Peroxide Oxidation of Pollutants with Different Lipophilicity, Catalysts 10 (2020) 1243.
[16] S.R.A. Santos, I.S. Jardim, H.A. Bicalho, I. Binatti, E.M.B. Sousa, A.M. Peres, R. R. Resende, E. Lorencon, Multifunctional catalysts based on carbon nanotubes and titanate nanotubes for oxidation of organic compounds in biphasic systems, J. Colloid Interface Sci. 483 (2016) 211–219.
[17] F.F. Roman, J.L. Diaz de Tuesta, A.M.T. Silva, J.L. Faria, H.T. Gomes, Carbon-Based Materials for Oxidative Desulfurization and Denitrogenation of Fuels: A Review, Catalysts 11 (2021) 1239.
[18] M.S. Kalmakhanova, J.L. Diaz de Tuesta, B.K. Massalimova, H.T. Gomes, Pillared clays from natural resources as catalysts for catalytic wet peroxide oxidation: Characterization and kinetic insights, Environ. Eng. Res. 25 (2019) 186–196.
[19] A. Santos Silva, M. Seitovna Kalmakhanova, B. Kabykenovna Massalimova, J. G. Sgorlon, Dd.T. Jose Luis, H.T. Gomes, Wet Peroxide Oxidation of Paracetamol Using Acid Activated and Fe/Co-Pillared Clay Catalysts Prepared from Natural Clays, Catalysts 9 (2019) 705.
[20] J.L. Diaz de Tuesta, M.C. Saviotti, F.F. Roman, G.F. Pantuzza, H.J.F. Sartori, A. Shinibekova, M.S. Kalmakhanova, B.K. Massalimova, J.M.T.A. Pietrobelli, G. G. Lenzi, H.T. Gomes, Assisted hydrothermal carbonization of agroindustrial byproducts as effective step in the production of activated carbon catalysts for wet peroxide oxidation of micro-pollutants, J. Environ. Chem. Eng. 9 (2021), 105004.
[21] R.S. Ribeiro, A.M.T. Silva, J.L. Figueiredo, J.L. Faria, H.T. Gomes, Catalytic wet peroxide oxidation: a route towards the application of hybrid magnetic carbon nanocomposites for the degradation of organic pollutants. A review, Appl. Catal. B: Environ. 187 (2016) 428–460.
[22] S. Navalon, M. Alvaro, H. Garcia, Heterogeneous Fenton catalysts based on clays, silicas and zeolites, Appl. Catal. B: Environ. 99 (2010) 1–26.
[23] M. Enterría, J.L. Figueiredo, Nanostructured mesoporous carbons: Tuning texture and surface chemistry, Carbon 108 (2016) 79–102.
[24] M. Martin-Martinez, B.F. Machado, P. Serp, S. Morales-Torres, A.M.T. Silva, J. L. Figueiredo, J.L. Faria, H.T. Gomes, Carbon nanotubes as catalysts for wet peroxide oxidation: The effect of surface chemistry, Catal. Today 357 (2020) 332–340.
[25] M. Martin-Martinez, R.S. Ribeiro, B.F. Machado, P. Serp, S. Morales-Torres, A.M. T. Silva, J.L. Figueiredo, J.L. Faria, H.T. Gomes, Role of nitrogen doping on the performance of carbon nanotube catalysts: a catalytic wet peroxide oxidation application, ChemCatChem 8 (2016) 2068–2078.
[26] H. Luo, H. Fu, H. Yin, Q. Lin, Carbon materials in persulfate-based advanced oxidation processes: The roles and construction of active sites, J. Hazard Mater. 426 (2022), 128044.
[27] R.P. Rocha, J. Restivo, J.P.S. Sousa, J.J.M. Órfão, M.F.R. Pereira, J.L. Figueiredo, Nitrogen-doped carbon xerogels as catalysts for advanced oxidation processes, Catal. Today 241 (2015) 73–79.
[28] A.D. Purceno, B.F. Machado, A.P. Teixeira, T.V. Medeiros, A. Benyounes, J. Beausoleil, H.C. Menezes, Z.L. Cardeal, R.M. Lago, P. Serp, Magnetic amphiphilic hybrid carbon nanotubes containing N-doped and undoped sections: powerful tensioactive nanostructures, Nanoscale 7 (2015) 294–300.
[29] A. Walther, A.H. Muller, Janus particles: synthesis, self-assembly, physical properties, and applications, Chem. Rev. 113 (2013) 5194–5261.
[30] B.P. Binks, P.D.I. Fletcher, Particles adsorbed at the oil−water interface: a theoretical comparison between spheres of uniform wettability and "Janus" particles, Langmuir 17 (2001) 4708–4710.
[31] B. Li, X. Sun, D. Su, Calibration of the basic strength of the nitrogen groups on the nanostructured carbon materials, Phys. Chem. Chem. Phys. 17 (2015) 6691–6694.
[32] B.F. Machado, R.R. Bacsa, C. Rivera-Cárcamo, P. Serp, Preparation of Few-Layer Graphene/Carbon Nanotube Hybrids Using Oxide Spinel Catalysts, C 5 (2019) 28.
[33] Z. Yue, W. Guo, J. Zhou, Z. Gui, L. Li, Synthesis of nanocrystilline ferrites by sol–gel combustion process: the influence of pH value of solution, J. Magn. Magn. Mater. 270 (2004) 216–223.
[34] M. Corrias, B. Caussat, A. Ayral, J. Durand, Y. Kihn, P. Kalck, P. Serp, Carbon nanotubes produced by fluidized bed catalytic CVD: first approach of the process, Chem. Eng. Sci. 58 (2003) 4475–4482.
[35] J.L. Diaz de Tuesta, A. Quintanilla, J.A. Casas, S. Morales-Torres, J.L. Faria, A.M. T. Silva, H.T. Gomes, The pH effect on the kinetics of 4-nitrophenol removal by CWPO with doped carbon black catalysts, Catal. Today 356 (2020) 216–225.
[36] M. Martin-Martinez, S. Álvarez-Torrellas, J. García, A.M.T. Silva, J.L. Faria, H. T. Gomes, Exploring the activity of chemical-activated carbons synthesized from peach stones as metal-free catalysts for wet peroxide oxidation, Catal. Today 313 (2018) 20–25.
[37] R.S. Ribeiro, R.O. Rodrigues, A.M.T. Silva, P.B. Tavares, A.M.C. Carvalho, J. L. Figueiredo, J.L. Faria, H.T. Gomes, Hybrid magnetic graphitic nanocomposites towards catalytic wet peroxide oxidation of the liquid effluent from a mechanical biological treatment plant for municipal solid waste, Appl. Catal. B 219 (2017) 645–657.
[38] M.H. Abraham, H.S. Chadha, G.S. Whiting, R.C. Mitchell, Hydrogen bonding. 32. An analysis of water-octanol and water-alkane partitioning and the Dlog P parameter of seiler, J. Pharm. Sci. 83 (1994) 1085–1100.
[39] R.S. Ribeiro, A.M.T. Silva, L.M. Pastrana-Martínez, J.L. Figueiredo, J.L. Faria, H. T. Gomes, Graphene-based materials for the catalytic wet peroxide oxidation of highly concentrated 4-nitrophenol solutions, Catal. Today 249 (2015) 204–212.
[40] A.A.S. Oliveira, A.R. Martins, R.V. Ferreira, I.T. Cunha, P. Serp, J.P. de Mesquita, F. C.C. Moura, N-doped carbon nanotubes grown on red mud residue: Hybrid nanocomposites for technological applications, Catal. Today 344 (2020) 247–258.
[41] A. Pacuła, K. Uosaki, R.P. Socha, E. Bielańska, P. Pietrzyk, M. Zimowska, Nitrogen-doped carbon materials derived from acetonitrile and Mg-Co-Al layered double hydroxides as electrocatalysts for oxygen reduction reaction, Electrochim. Acta 212 (2016) 47–58.
[42] Z.N. Tetana, S.D. Mhlanga, G. Bepete, R.W.M. Krause, N.J. Coville, The synthesis of nitrogen-doped multiwalled carbon nanotubes using an Fe-Co/$CaCO_3$ catalyst, S. Afr. J. Chem. 65 (2012) 39–40.
[43] N.V. Lemesh, P.E. Strizhak, Synthesis of multi-walled carbon nanotubes with controlled inner and outer diameters by ethylene decomposition over Ni/MgO and Co/MgO catalysts, Mater. Sci. -Pol. 36 (2018) 739–747.
[44] A.H. Labulo, N.P.D. Ngidi, B. Omondi, V.O. Nyamori, Physicochemical properties of nitrogen-doped carbon nanotubes from metallocenes and ferrocenyl imidazolium compounds, J. Organomet. Chem. 868 (2018) 66–75.
[45] J.L. Figueiredo, M.F.R. Pereira, The role of surface chemistry in catalysis with carbons, Catal. Today 150 (2010) 2–7.
[46] E.A. Arkhipova, A.S. Ivanov, N.E. Strokova, S.A. Chernyak, A.V. Shumyantsev, K. I. Maslakov, S.V. Savilov, V.V. Lunin, Structural evolution of nitrogen-doped carbon nanotubes: From synthesis and oxidation to thermal defunctionalization, Carbon 125 (2017) 20–31.
[47] M.L. García-Betancourt, J.L. Fajardo-Díaz, R. Galindo, R. Fuentes-Ramírez, F. López-Urías, E. Muñoz-Sandoval, Holey nitrogen-doped multiwalled carbon

nanotubes from extended air oxidation at low-temperature, Appl. Surf. Sci. 524 (2020), 146546.
[48] J.H. Lehman, M. Terrones, E. Mansfield, K.E. Hurst, V. Meunier, Evaluating the characteristics of multiwall carbon nanotubes, Carbon 49 (2011) 2581–2602.
[49] K. Voitko, A. Toth, E. Demianenko, G. Dobos, B. Berke, O. Bakalinska, A. Grebenyuk, E. Tombacz, V. Kuts, Y. Tarasenko, M. Kartel, K. Laszlo, Catalytic performance of carbon nanotubes in H_2O_2 decomposition: experimental and quantum chemical study, J. Colloid Interface Sci. 437 (2015) 283–290.
[50] M.T. Pinho, R.S. Ribeiro, H.T. Gomes, J.L. Faria, A.M.T. Silva, Screening of activated carbons for the treatment of highly concentrated phenol solutions using catalytic wet peroxide oxidation: the effect of iron impurities on the catalytic activity, Catalysts 10 (2020) 1318.
[51] N. Inchaurrondo, J. Cechini, J. Font, P. Haure, Strategies for enhanced CWPO of phenol solutions, Appl. Catal. B. 111–112 (2012) 641–648.
[52] X. Ou, H. Daly, X. Fan, S. Beaumont, S. Chansai, A. Garforth, S. Xu, C. Hardacre, High-ionic-strength wastewater treatment via catalytic wet oxidation over a $MnCeO_x$ catalyst, ACS Catal. 12 (2022) 7598–7608.
[53] J.L. Díaz de Tuesta, C. García-Figueruelo, A. Quintanilla, J.A. Casas, J.J. Rodriguez, Application of high-temperature Fenton oxidation for the treatment of sulfonation plant wastewater, J. Chem. Technol. Biotechnol. 90 (2015) 1839–1846.
[54] S.-P. Sun, A.T. Lemley, p-Nitrophenol degradation by a heterogeneous Fenton-like reaction on nano-magnetite: Process optimization, kinetics, and degradation pathways, J. Mol. Catal. A Chem. 349 (2011) 71–79.
[55] C.S.D. Rodrigues, R.A.C. Borges, V.N. Lima, L.M. Madeira, p-Nitrophenol degradation by Fenton's oxidation in a bubble column reactor, J. Environ. Manag. 206 (2018) 774–785.
[56] S. Chaliha, K.G. Bhattacharyya, P. Paul, Oxidation of 4-nitrophenol in water over Fe(III), Co(II), and Ni(II) impregnated MCM41 catalysts, J. Chem. Technol. Biotechnol. 83 (2008) 1353–1363.
[57] L. Zhao, J. Ma, Z.-z Sun, Oxidation products and pathway of ceramic honeycomb-catalyzed ozonation for the degradation of nitrobenzene in aqueous solution, Appl. Catal. B: Environ. 79 (2008) 244–253.
[58] F. Mijangos, F. Varona, N. Villota, Changes in solution color during phenol oxidation by Fenton reagent, Environ. Sci. Technol. 40 (2006) 5538–5543.
[59] F.D. Kopinke, A. Georgi, What Controls Selectivity of Hydroxyl Radicals in Aqueous Solution? Indications for a Cage Effect, J. Phys. Chem. A 121 (2017) 7947–7955.
[60] C. Zhang, C. Jia, Y. Cao, Y. Yao, S. Xie, S. Zhang, H. Lin, Water-assisted selective hydrodeoxygenation of phenol to benzene over the Ru composite catalyst in the biphasic process, Green. Chem. 21 (2019) 1668–1679.
[61] C. Li, H. Cai, B. Zhang, W. Li, G. Pei, T. Dai, A. Wang, T. Zhang, Tailored one-pot production of furan-based fuels from fructose in an ionic liquid biphasic solvent system, Chin. J. Catal. 36 (2015) 1638–1646.
[62] C. Jia, C. Zhang, S. Xie, W. Zhang, Z. Wang, H. Lin, One-pot production of jet fuels from fatty acids and vegetable oils in biphasic tandem catalytic process, Fuel 302 (2021), 121060.
[63] J. Zhan, R. Hu, X. Luo, C. Zhang, G. Luo, J. Fan, J.H. Clark, S. Zhang, Highly selective conversion of phenol to cyclohexanol over Ru/Nb_2O_5-*n*C18PA catalysts with increased acidity in a biphasic system under mild conditions, Green. Chem. 24 (2022) 1152–1164.
[64] M. Martin-Martinez, M.F.F. Barreiro, A.M.T. Silva, J.L. Figueiredo, J.L. Faria, H. T. Gomes, Lignin-based activated carbons as metal-free catalysts for the oxidative degradation of 4-nitrophenol in aqueous solution, Appl. Catal. B 219 (2017) 372–378.
[65] R.S. Ribeiro, A.M.T. Silva, J.L. Figueiredo, J.L. Faria, H.T. Gomes, The role of cobalt in bimetallic iron-cobalt magnetic carbon xerogels developed for catalytic wet peroxide oxidation, Catal. Today 296 (2017) 66–75.